Bioluminescence dynamics in single germinating bacterial spores reveal metabolic heterogeneity

Zak Frentz and Jonathan Dworkin*

Department of Microbiology and Immunology, College of Physicians and Surgeons, Columbia University, New York, NY 10032

* Corresponding author,

Abstract

Spore-forming bacteria modulate their metabolic rate by over 5 orders of magnitude as they transition between dormant spores and vegetative cells, and thus represent an extreme case of phenotypic variation. During environmental changes in nutrient availability, clonal populations of spore-forming bacteria exhibit individual differences in cell fate, timing of phenotypic transitions, and gene expression. One potential source of this variability is metabolic heterogeneity, but this has not yet been measured, as existing single-cell methods are not easily applicable to spores due to their small size and strong autofluorescence. Here, we use the bacterial bioluminescence system and a highly sensitive microscope to measure metabolic dynamics in thousands of *B. subtilis* spores as they germinate. We observe and quantitate large variations in the bioluminescence dynamics across individual spores that can be decomposed into contributions from variability in germination timing, the amount of endogenously produced luminescence substrate, and the intracellular reducing power. This work shows that quantitative measurement of spore metabolism is possible and thus it opens venues for future study of the thermodynamic nature of dormant states.

Introduction

Some bacteria respond to nutrient depletion by differentiating from growing, vegetative cells into spores that can survive extreme temperatures, radiation, and long periods without nutrients, while retaining the ability to germinate and reinitiate growth in the presence of sufficient nutrients [1-3]. One of the most remarkable aspects of spore-forming bacteria is the extreme reduction of their metabolic rate, by at least 5 orders of magnitude, during sporulation [4]. Metabolic dormancy and resistance allow spores to survive for long times in harsh environments, which typically fluctuate. Dynamically sensing the environment requires energy expenditure [5], and thus is likely difficult for spores given their low or nonexistent metabolism. Therefore, sporulating populations must adapt to fluctuating environments through other strategies, such as phenotypic diversification, or "bet-hedging" [6, 7].

Significant heterogeneity is observed in populations during both the sporulation and germination transitions. For example, after nutrient limitation, only a portion of vegetative cells commit to sporulation, while other cells either lyse or survive in the vegetative state by using secondary metabolites [8]. The time at which a vegetative cell sporulates varies significantly within a population, and this time correlates with the time at which the ensuing spore germinates and in its ability to resume growth in various nutrients [9]. Spores germinate in reponse to low concentrations of nutrients at variable times [7], and this variability is partially explained by the number of germinant receptors in each spore [10]. Even in the absence of germinants, a small fraction of spores germinates spontaneously [11, 12]. These phenomena of phenotypic heterogeneity have been linked to variations in gene expression [8, 9, 12, 13]. However, the remarkable dynamics of metabolism during sporulation and germination have not been measured in individual cells, due to lack of a suitable technique.

The dynamics of energy metabolism can be measured in single vegetative bacteria using several *in vivo* methods, most of which are based on fluorescence [14]. These are difficult to apply to spores due to their strong autofluorescence, primarily from calcium dipicolinate, NADH, and

flavins [15, 16]. The intracellular redox potential drives all pathways of energy metabolism other than fermentation [17, 18], and has been measured *in vivo* in single bacterial cells using a custom-fabricated microelectrode coupled to an optical trap [19]. However, this technique requires a specialized device, operates in anaerobic conditions, and only measures a small number of cells.

An alternative approach uses the bacterial luminescence system [20]. An enzyme, luciferase, encoded by the *luxAB* genes, catalyzes the light-emitting oxidation of a substrate, luciferin, which can be supplied exogenously or synthesized endogenously by expression of the *luxCDE* genes. The oxidation reaction's rate depends on the reduced form of the electron transporter flavin mononucleotide ($FMNH_2$), whose concentration is determined by the intracellular reducing power [21]. Thus, the rate of light production directly relates to the redox potential. In addition, since the emission of light occurs without external illumination, bioluminescent techniques can be considered "zero background", and therefore offer improved sensitivity as compared to fluorescent techniques. Here we describe a microscope designed to capture the dynamics of bioluminescence emitted by single cells, which we used to non-invasively assay metabolic activity of single germinating spores of *Bacillus subtilis*.

Results

Bioluminescence microscopy of single spores

To date, the bioluminescence dynamics of sporulating and germinating cells have been measured only in populations, typically using a photomultiplier tube for photon counting [22, 23]. A *B. subtilis* strain that expresses the *lux* genes under a sporulation-specific promoter (P_{sspB}) produces spores that contain a sufficient number of luciferase enzymes to emit detectable light only upon germination [23]. Prior to germination, spores do not emit detectable light, presumably due to their dormant metabolic state.

The feasibility of measuring bioluminescence dynamics in single germinating spores is determined by the rate of photon emission, which must be sufficiently high to be resolved over

77 measurement noise. This rate increases with higher expression of the *luxABCDE* genes, as has
78 recently been achieved in *B. subtilis* by modifying the ribosomal binding sites upstream of each
79 gene [24]. The rate of bioluminescent photon emission at the population level has been reported
80 in relative light units, or RLUs [24, 25], which are defined differently for various devices. RLUs can
81 be converted to units of photons per time per cell by calibration with a luminescent standard [26],
82 although this calibration has not been included in the published results. As a rough guide,
83 microscopy of individual metabolically active *Escherichia coli*, *Synechoccocus elongatus*, *Vibrio*
84 *fischeri*, and *Vibrio harveyi* cells expressing the lux system typically measures ~60 photons min^{-1}
85 $cell^{-1}$ [27-29]. Our preliminary analysis suggested that a microscope utilizing recent improvements
86 in CCD technology could resolve bioluminescence signals as dim as 1 photons min^{-1} $spore^{-1}$ (SI
87 Appendix).

88 We therefore constructed a custom microscope for measuring the dynamics of
89 bioluminescence in single spores (Fig. 1A, Materials and Methods). The microscope includes an
90 optical path for bright field imaging, which is used to localize spores and measure their refractility,
91 as described below. The setup consists of an inverted microscope with a high-NA 63X objective
92 and a cooled, back-illuminated CCD camera. We used 10 min exposure times, sufficient to
93 resolve germination dynamics while achieving sensitivity to permit measurements from single
94 germinating spores. Over a period of 10 min, Brownian motion displaces a spore by a root-mean-
95 square displacement of approximately 50 μm. To prevent such displacements, we trapped the
96 spores by using hydrophobic glass coverslips. With this method, the displacement of spores over
97 10 min periods was below the optical resolution of the bright field images (<160 nm). The sample
98 was held in a perfusion chamber, which dynamically controlled the chemical environment (Fig.
99 1B) , and the temperature at the sample was controlled to ±0.05 ℃ by an air-to-air heat exchanger.

100 We initially investigated the dynamics of bioluminescence emitted by single *B. subtilis*
101 spores as they germinated in response to L-alanine. These spores (JDB3780) expressed the
102 *luxABCDE* genes under the control of a sporulation-specific promoter. A field of approximately

103 900 spores was imaged in bright field and luminescence every 10 min for 1.5 h (Fig. 1C). Prior to
104 the induction of germination, the dormant spores appeared dark, with high contrast, and produced
105 no resolvable luminescence signal (Figs. 1D and E). L-alanine was added to the perfusion media
106 at a concentration of 100 μM, and the ensuing germination response was recorded for 15 h.

107 After an initial lag following the addition of L-alanine, most spores showed a significant
108 decrease of contrast in bright field, and many produced luminescence well above the noise
109 background (Figs. 1F and G). The predominant source of measurement noise was sensor read
110 noise; we found that its contribution could be reduced significantly by applying a temporal low-
111 pass filter with a cutoff period of 36 min (SI Appendix). Sensor read noise has a Gaussian
112 distribution, and can therefore produce estimated photon counts that are negative [30]. We
113 determined that the technique had a sensitivity limit of 0.4 photons min^{-1} $spore^{-1}$ (SI Appendix).

114 The dynamics of individual spores in the bright field and luminescence images were
115 analyzed, resulting in time series of bright field contrast and estimated luminescent photon counts
116 for individual spores (Figs. 1H and I). Rapid loss of contrast after the addition of L-alanine was
117 evident in most spores, indicating an early event in germination, namely, the release of calcium
118 dipicolinate from the spore [31]. Spores differed significantly in their time of germination (Fig. 1H)
119 and in their bioluminescence signals (Fig. 1I).

120

121 **Bioluminescence dynamics are synchronized with germination time**

122 In order to compare the measurements in the microscope to an established method, we used a
123 96-well plate reader to measure the population-averaged bioluminescence dynamics of spores
124 germinating in response to the addition of L-alanine at 5 different concentrations (1 μM, 10 μM,
125 100 μM, 1 mM, and 10 mM) (Fig. 2A). Time-lapse experiments were performed in the microscope
126 setup at the same L-alanine concentrations, and the population-averaged bioluminescence
127 dynamics were calculated (Fig. 2B). The dynamics as measured by both methods shared some
128 features: Signal intensity generally increased with increasing L-alanine concentration, from total

129 darkness at 1 μM, to a peak level at 1 mM, then decreased slightly at 10 mM (Fig. 2C). The L-
130 alanine concentration also affected the temporal patterns of the dynamics: In the measurements
131 performed with the microscope, a peak in the bioluminescence signal was evident approximately
132 1 h after germination with 10 mM, 1 mM, and 100 μM L-alanine, but this peak was not observed
133 following germination with 10 μM L-alanine (Fig. 2B). Although much less pronounced, this early
134 peak was also apparent in the plate reader measurements after germination with 10 mM and 1
135 mM L-alanine; with 100 μM and 10 μM L-alanine, no peak was resolved, but a "shoulder" at 40
136 min was apparent in both conditions (Fig. 2A). The primary difference in the dynamics measured
137 by the two methods was the much higher intensity of the early peak measured in the microscope.
138 We observed similar differences caused by varying the spore density in the plate reader
139 experiments (Fig. S1), which are likely due to chemical interactions between germinating spores.
140 This effect can explain the differences observed between the dynamics measured in the plate
141 reader, at a density of 3×10^7 spores ml^{-1}, and in the microscope, at a density of less than 10^5
142 spores ml^{-1}.

143 The observed population-averaged bioluminescence dynamics arise from temporal
144 fluctuations in individual spores as well as variability in the population, and these two sources can
145 be separated using the single-spore technique. In particular, individual spores germinate at
146 different times, with large variability observed at low L-alanine concentrations [32]. With
147 automated image analysis, we identified the time τ_g of rapid contrast loss in each germinating
148 spore (SI Appendix), and interpreted τ_g as the time at which each spore started germination. We
149 considered the statistics of germination dynamics by calculating the fraction of the population that
150 had not yet germinated by time t: This is the tail distribution function of germination time, $P(\tau_g>t)$
151 (Fig. 3A). At L-alanine concentrations of 100 μM and higher, most spores germinated within 1 h
152 of induction, and over 99% of spores germinated within 13 h. In contrast, spores germinated much
153 more slowly in response to the addition of 10 μM L-alanine, with only half of all spores germinating

154 within 13 h. For the 1 μM L-alanine concentration, we did not observe any germination for spores
155 up to 82 h after induction.

156 The distributions of germination time τ_g reveal significant variability in the population of
157 spores, especially evident in the 10 μM L-alanine condition. To investigate the relationship
158 between this variability and the bioluminescence dynamics, we considered the bioluminescence
159 of each cell as a function of time elapsed since germination: $\phi_g(t) = \phi(t\text{-}\tau_g)$, defined for all spores
160 that germinated during the observation interval. Note that the germination time τ_g was determined
161 exclusively by the bright field images, through a procedure that was independent of the
162 bioluminescence dynamics (SI Appendix). The population averages of $\phi_g(t)$ in each germination
163 condition indicate significant synchronization of the bioluminescence dynamics with the time of
164 germination, as evidenced by the qualitatively similar temporal patterns in the 4 conditions for
165 which germination was observed (Fig. 3B). In particular, we observe remarkable alignment in the
166 timing of a primary peak at $t \approx 40$ min, the appearance of a secondary peak between $t = 2$ h and
167 $t = 3$ h, and similar profiles of signal attenuation at later times, possibly due to degradation of the
168 lux enzymes (Fig. S2).

169

170 **Bioluminescence varies significantly across spores**

171 Aligning the dynamics to the time of germination τ_g accounted for the occurrence and timing of
172 germination as a source of the variability observed in the bioluminescence dynamics. Significant
173 variability remained in the aligned dynamics $\phi_g(t)$ (Fig. 4A). We analyzed the variability of $\phi_g(t)$
174 over spores to answer two questions: First, what are the temporal correlations of the
175 bioluminescence dynamics in individual spores? Second, how much of the variability in
176 bioluminescence is due to variations in the factors that affect the reaction chemistry, namely, the
177 redox potential, luciferin concentration, and luciferase copy number?

178 To analyze temporal correlations in the bioluminescence dynamics, we calculated the
179 temporal covariance matrix $C(s,t)$ from the photon counts ϕ_g at times s and t (SI Appendix). This

180 calculation was performed over all germinating spores from the 4 concentrations of L-alanine for
181 which germination was observed. The covariance matrix was analyzed using principal component
182 analysis (PCA): PCA applied to time series in this manner is often referred to as empirical
183 orthogonal function analysis [33]. The first principal component explained 30% of the variance
184 over individuals, while additional components each explained only a few percent of the total
185 variance (Fig. S3). Therefore, we focused on the pattern of correlations described by the first
186 component, which had temporal structure similar to the population-averaged dynamics (Fig. 4B).
187 This similarity indicates that the dynamics in most spores were well-described by the mean
188 dynamics multiplied by a coefficient specific to each spore, which we call its amplitude. This simple
189 mode of variation was useful for quantifying the contributions from different sources, as described
190 below.
191

192 **Bioluminescence variability arises from variations in redox potential and luciferin**
193 **concentration**

194 Besides the timing of germination, several factors could contribute to variability in the
195 bioluminescence dynamics. The redox potential and concentration of luciferin in each cell are two
196 obvious candidates. To investigate these, we performed an experiment with fumarate added to
197 the germination buffer, in order to drive the citric acid cycle and thus increase the intracellular
198 redox potential. In a second experiment, decanal was added as an exogenous luciferin. In a third
199 experiment, both fumarate and decanal were added to the germination buffer. Spores germinated
200 in response to the addition of 1 mM L-alanine. We calculated the population-averaged
201 bioluminescence dynamics and performed PCA for each data set independently (Figs. 4C-E).

202 In the presence of fumarate, the population-averaged bioluminescence dynamics $\langle \phi_g(t) \rangle$
203 exhibited 2 distinct peaks, approximately 40 min and 3 h after germination (Fig. 4C). These
204 dynamics appear to be similar to those observed in germination buffer without fumarate (Fig. 4B),
205 with two major differences: The addition of fumarate increased the intensity of the second peak,

206 and strongly attenuated the spore-to-spore variability during the first peak, as indicated by the
207 disappearance of the first peak from the first principal component. The addition of exogenous
208 luciferin (decanal), both with and without fumarate, resulted in population-averaged
209 bioluminescence dynamics with a single peak, occurring approximately 40 min after germination,
210 with intensity approximately 10-fold higher than the initial peak observed in the absence of
211 exogenous luciferin (Figs. 4D and 4E).

212 In all conditions, PCA revealed a single significant component of variation (Fig. S3), and
213 in each condition, this mode's eigenvector was strongly correlated with the average dynamics
214 (Figs. 4B-E). Thus the primary mode of variation in all conditions was variability in amplitude. This
215 simple pattern facilitates the quantitation of variability, since the contribution of each spore's signal
216 to the total variability can be summarized by a single variable: the signal amplitude. Thus we
217 calculated for each germinating spore the total number of photons counted during the 12 h
218 following germination, n_g.

219 The mean value of n_g varied significantly in different conditions. Therefore, to compare
220 variability in n_g across conditions, we considered the ratio of the standard deviation to the mean,
221 $\eta=\sigma_{n_g}\langle n_g\rangle^{-1}$, also known as the coefficient of variation. We also considered the asymmetry in the
222 distribution of n_g by calculating its skew, γ. The estimated statistics are summarized in Table 1.
223 Variability was high for spores germinating in the absence of exogenous factors (η=160%), and
224 the distribution of n_g had strong positive skew (γ=3.3). The addition of fumarate significantly
225 decreased the coefficient of variation and the skew (η=125%, γ=1.4). The addition of decanal
226 reduced the variability and skew more strongly (η=55%, γ=0.6). The addition of both fumarate
227 and decanal had the largest effect (η=39%, γ=0.32). We conclude that the large amount of
228 variability in bioluminescence signal observed in spores germinating in the absence of exogenous
229 factors was predominantly due to variability in both intracellular luciferin concentration and redox
230 potential.

231 The bioluminescence dynamics following germination are influenced by metabolic
232 changes that occur early in germination, including the initiation of electron transport [23, 34]. In
233 addition to inducing germination, L-alanine may also fuel energy metabolism [9]. To investigate
234 this possibility, we considered the photon counts n_g from spores germinating in response to 4
235 concentrations of L-alanine, in germination buffer (Fig. S4). The population-average $\langle n_g \rangle$
236 increased 2-fold as the L-alanine concentration increased from 10 μM to 1 mM, then decreased
237 at 10 mM. The variation in amplitude with L-alanine concentration arose primarily from a
238 subpopulation of the brightest spores (Fig. S5). The weak, non-monotonic dependence of the
239 bioluminescence signal on L-alanine concentration indicates that exogenous L-alanine does not
240 significantly drive energy metabolism in germinating spores.
241

242 **Discussion**

243 The spore is an extreme phenotypic state that allows an organism to survive extended periods of
244 starvation, drought, and radiation. Metabolism decreases to extremely low levels during
245 sporulation, then rapidly increases during germination. Laboratory studies of populations
246 undergoing the sporulation and germination transitions have also revealed large amounts of
247 variability over individuals, suggesting that phenotypic diversification in natural spore-forming
248 populations is a bet-hedging strategy for surviving in fluctuating environments. It is therefore
249 important to study metabolic dynamics in individual spores.

250 No previously described methods for quantifying metabolic dynamics in single cells are
251 applicable to *Bacillus* spores. Therefore, we developed a microscopic technique for this purpose,
252 using a bioluminescent reporter for the intracellular redox potential. In this paper, we measured
253 bioluminescence dynamics from individual spores germinating in response to L-alanine, which is
254 both a germinant and a potential nutrient. Comparing the bioluminescence dynamics measured
255 in individuals to the population average, we exposed significant variability in the population. A
256 major source of variability was shown to be associated with differences in the timing of

257 germination. We could remove this contribution from the bioluminescence dynamics by
258 simultaneously using bright field microscopy to precisely determine the time of germination of
259 each spore. The bioluminescence dynamics could then be analyzed for its temporal correlations.
260 The analysis indicated that the primary mode of variation was associated with the amplitude of
261 the bioluminescence signal produced by each spore.

262 By performing experiments at different concentrations of L-alanine, we were able to show
263 that it was not a major source of variations in bioluminescence amplitude, suggesting that
264 metabolism in germinating spores was driven not by L-alanine, but rather by endogenous energy
265 sources stored during sporulation. Through the addition of exogenous nutrients (fumarate) and
266 bioluminescence substrate (luciferin), we were able to decompose the variability in
267 bioluminescence amplitude into two main sources: the intracellular redox potential and luciferin
268 concentration. Both of these sources relate to energy metabolism, as the redox potential drives
269 ATP synthesis, and the biosynthesis of luciferin depends on both ATP and NADPH [35]. Our
270 results show that we can begin to understand the metabolic transitions between the growing and
271 dormant states at the level of single cells.

272 We foresee two important extensions of the current work. First, one can study the
273 variability of metabolic dynamics in fluctuating environments. Vegetative cells can be tracked as
274 they sporulate in response to experimentally imposed starvation, and later germinate and outgrow
275 in response to nutrients [9]. By simultaneously measuring the bioluminescence dynamics in this
276 type of experiment, we can study the correlations between spores' timing of sporulation, timing of
277 germination, ability to outgrow, and metabolic state. Environments also fluctuate due to biotic
278 interactions. Bacterial spores contain high concentrations of calcium dipicolinate, a compound
279 that affects resistance and dormancy, but also induces germination in dormant spores [36].
280 Because spores release large amounts of calcium dipicolinate during germination [37], the local
281 concentration of spores can affect their germination behavior. Such interactions may explain the
282 differences we observed in the bioluminescence dynamics with respect to spore density (Figs. 2A

283 and B, Fig. S1). Interactions between spores and their effects on metabolism could be studied
284 systematically by analyzing the spatial statistics of germination timing and bioluminescence.

285 A second extension is to study the thermodynamic nature of dormant states. The
286 maintenance of order in living matter seems to require energy expenditure, in order to counteract
287 spontaneously occurring degradation [38, 39]. Therefore, a central question arises: What are the
288 energetic limits for survival? This question has primarily been studied in microbial communities
289 from low-energy environments, including deep sediments, permafrost, and subglacial lakes [40-
290 42]. Metabolic activity in such environments, averaged over the community, has been found to be
291 reduced by 5 to 6 orders of magnitude compared to the state of growth when nutrients are
292 supplied [40, 41]. These low metabolic rates are approximately equal to the energetic costs of
293 repairing molecular damage to proteins and DNA at the corresponding temperatures [41, 42].
294 However, these analyses included contributions from cells with metabolic activity that was
295 potentially significantly lower than the population average, including dormant spores [43].
296 Therefore, spores likely represent the most extreme case of metabolic dormancy in nature.

297 Most studies of metabolism in dormant spores have not detected activity [44-47].
298 Extraodinarily sensitive measurements of metabolism in populations of dormant spores using
299 radiochemical labelling of metabolites did detect activity, reduced by over 5 orders of magnitude
300 compared to the vegetative state [4]. However, the detected metabolism could have been due to
301 a rare subpopulation of germinating spores [4, 11, 12], and therefore can serve only as an upper
302 bound on the rate of metabolic activity in dormant spores. By resolving individual spontaneous
303 germination events, bioluminescence microscopy could achieve unprecedented sensitivity. The
304 intensity of bioluminescence is linear in the concentration of $FMNH_2$ at low concentrations [48],
305 so its utility as a metabolic reporter should extend to cells with very low metabolic rates, such as
306 dormant spores. A measurement on a single spore at a single time point with signal-to-noise ratio
307 ξ can be averaged over N individuals and T time points to produce a bulk measurement with
308 signal-to-noise ratio $\xi(NT)^{1/2}$. For our method applied to germinating spores, ξ is ~20 (SI

Appendix). This suggests that bioluminescence measurements could achieve sensitivity concomitant with a 10^5-fold reduction in signal compared to germinating spores by measuring, for example, a population of 10^4 dormant spores over an interval of 18 d, which is feasible using the setup described here.

A possible mechanism for long-term survival without any metabolic activity is the formation of a thermodynamically metastable state. The glassy state is an example of metastability that has been invoked to explain spore dormancy [49, 50], as macromolecules in a glass change conformation extremely slowly [51]. Therefore, a glassy environment could in principle reduce the rate of molecular damage to proteins and DNA, while also reducing the activity of metabolic enzymes and thus causing dormancy. Direct characterization of glassiness in spores is difficult, as the internal structure of the spore is highly heterogeneous [52]. Instead, one can study a feature of spores from the perspective of metastability, namely, the statistics of spontaneous germination and its dependence on environmental conditions such as temperature. This approach should be possible with our technique, which would also quantify possible differences in metabolism between spores germinating spontaneously and those germinating in response to nutrients.

Acknowledgments

We thank members of the Dworkin and S. Leibler labs for helpful discussions. ZF was supported by a grant from Simons Foundation to S. Leibler through Rockefeller University Grant 345430 and JD was supported by NIH GM122146.

331 **Materials and Methods**

332 **Strains**

333 JDB3780 (168 *trpC2 sacA::*P_{sspB}*-luxABCDE::cm*) was constructed by transforming genomic DNA

334 from RL4921 (PY79 *sacA::*P_{sspB}*-luxABCDE::cm*) into JDB1772 (168 *trpC2).*

335

336 **Sporulation protocol**

337 Spores were prepared in Difco sporulation media (DSM). Single colonies grown on LB agar were

338 used to inoculate 3 ml cultures in test tubes. Cultures were grown with shaking at 30 ℃ for 3 h.

339 30 µl aliquots were used to inoculate 30 ml cultures in baffled flasks. After growing with shaking

340 at 30 ℃ for 36 h, spores were purified by spinning at 5,400 g for 10 min at 4 ℃ and resuspending

341 in sterile water. Cold water washes were repeated 4 times, yielding samples that were

342 predominantly refractile spores (>90%). Samples were stored at 4 ℃.

343

344 **Plate reader assay**

345 To assay bioluminescence dynamics in response to various concentrations of L-alanine, dormant

346 spores (JDB3780) were suspended in 25 mM Tris-HCl buffer at pH 8.2, at a density of 3×10^{7}

347 spores ml^{-1}. 200 µl of spore suspension was pipetted into wells of a 96-microwell plate (Nunc

348 236108). In order to avoid both signal contamination from neighboring wells as well as the

349 influence of thermal gradients, wells were filled only in the plate interior, in a checkerboard pattern.

350 2 µl of L-alanine solutions at concentrations between 1 M and 1 mM were added to the appropriate

351 wells. Each germinant condition was prepared in 3 replicate wells. Three wells with 200 µl of

352 buffer were included as blanks. The plate was sealed with a gas permeable, partially adhesive

353 film (Uniscience C20613201), and positioned within the plate reader (Perkin Elmer Wallac Victor^{2}

354 1420-011). Luminescence measurements were made without an optical filter, normal aperture

355 setting, and 10 s integration time. The temperature was maintained at 30 ± 1 ℃. Between

356 luminescence readings, the plate was shaken orbitally for 10 s with a 2 mm diameter at the slow
357 speed setting. The plate reader assay of bioluminescence in the presence of chloramphenicol
358 was performed using a similar procedure, with spores of JDB3785 suspended at a density of
359 1.2×10^{8} spores ml^{-1} and germinated with 1 mM L-alanine.
360

361 **Reagents and Media**

362 All germination experiments were conducted in germination buffer (25 mM Tris-HCl, pH 8.2).
363 Decanal was dissolved at a concentration of 15 mM in a 1:1 solution of methanol and water.
364

365 **Microscopy**

366 Sample preparation

367 All sample preparation was conducted with sterile technique at the bench.

368 Adhesion of dormant and germinating spores to glass coverslips was improved by
369 rendering the glass surface hydrophobic. Coverslips were treated with vapor deposition of
370 hexamethyldisilazane (Alfa Aesar L16519AE) in a sealed chamber for 1 h, followed by baking at
371 80 ℃ for 1 h.

372 Agarose pads were prepared by pipetting 700 µl of molten 4% low-melt agarose (Fisher
373 BP165-25) between two 22 mm diameter glass coverslips. After 1 h at room temperature, the
374 agarose pad was exposed by removing the top coverslip, and dried for 5 min.

375 Prior to spotting the pad, dormant spores were washed twice with water (5400 g, 10 min,
376 4 ℃). 2 µl of the spore suspension was pipetted onto the center of the dried pad, and the spot
377 was allowed to completely evaporate (~10 min). The pad was then separated from the bottom
378 coverslip, and inverted onto a hydrophobic glass coverslip (30 mm diameter, #1.5 thickness,
379 Bioptechs). The coverslip-bonded pad was left to evaporate for 30 min, then assembled into the
380 bottom of the perfusion chamber (Bioptechs, ICD with heated lid, gas and media perfusion).

381 Molten 4% low-melt agarose was added to the exposed portion of the coverslip, and allowed to
382 gel for 30 min. Creating a contiguous layer of agarose in this manner was found to attenuate
383 coverslip bounce resulting from the perfusion flow.
384
385 Perfusion
386 A peristaltic pump (Cole-Parmer, Masterflex L/S digital miniflex, dual-channel) was used to draw
387 media from a reservoir bottle, through sterile tubing (Cole-Parmer, C-Flex #13, i.d. 0.8 mm), into
388 the perfusion chamber, and finally into a waste reservoir bottle. Tubing was connected with
389 standard Luer locks, and the bottle openings were wrapped tightly with Parafilm and covered in
390 aluminum foil. At the beginning of each experiment and whenever the medium was changed (for
391 example, when germinant was added), the flow was primed at 1 ml min^{-1}. Otherwise, the flow rate
392 was 50 µl min^{-1}.
393 Prior to conducting each imaging experiment, the perfusion tubing was sterilized by
394 flowing 100 ml 20% bleach, followed by 100 ml isopropanol, followed by 5 subsequent bottles
395 containing 250 ml sterile, purified water (Milli-Q). The perfusion chamber was cleaned by rinsing
396 with 20% bleach, isopropanol, and distilled water, then air dried.
397
398 Imaging
399 The imaging setup consisted of an inverted optical microscope (Zeiss Axiovert 135), a 63X 1.4
400 NA oil immersion DIC objective (Zeiss 1113-108) operated without the Wollaston prism, and a
401 sensitive, back-illuminated, cooled CCD camera (Princeton Instruments, PIXIS 1024B).
402 A collimated, 445 nm LED (Thorlabs, Solis-445C) was used as external illumination for
403 bright field imaging. For acquisition of bright field images, the LED was pulsed for 50 ms at low
404 current (40 mA), and was otherwise fully off.
405 Autofocus was maintained via a pupil obscuration method applied to an infrared (780 nm)
406 beam reflected from the glass-media interface (Applied Scientific Instrumentation, CRISP). The

407 defocus detector controlled the focal position through a DC servo motor connected to the
408 mechanical focusing shaft of the microscope (Applied Scientific Instrumentation, MFC-2000).
409 Luminescence images were acquired with 10 min exposure time. The readout was
410 performed at 100 kHz (read noise 3.56 e^-), high gain (1.00 e^- ADU^{-1}), and with 2x2 binning. The
411 CCD was cooled to -65 ℃ with a combination of thermoelectric and low-vibration liquid cooling
412 (Princeton Instruments, CoolCUBE II). At this temperature, the dark current was measured at 10^{-3}
413 e^- $pixel^{-1}$ s^{-1}.
414 The microscope and camera were enclosed inside a box made of styrofoam-lined black
415 plastic. Exterior edges and corners of the box were covered with opaque black fabric and taped.
416 A removable styrofoam-lined plastic panel provided access to the microscope and sample holder,
417 and was held in place during data acquisition with Velcro straps and metal L-brackets. The
418 temperature within the box was controlled by a thermoelectric device (TE Technology, AC-220),
419 coupled to a PID feedback device (TE Technology, TC-720) monitoring a thermistor placed as
420 close as possible to the perfusion chamber. The interior temperature of the box was maintained
421 at 30±0.05 ℃. The entire imaging apparatus was supported by a vibration-damped optical table,
422 situated in a temperature-controlled room (28±0.1 ℃).
423
424 **Image analysis and statistics**
425 See SI Appendix.
426

427 **Table**

media	#spores	mean: $\langle n_g \rangle$ [photons]	coefficient of variation: η	skew: γ
germination buffer only	11,882	1,300±19	161% [154%, 169%]	3.326±0.022
germ. buffer +0.4% fumarate	1,976	2,862±81	125% [117%, 137%]	1.449±0.055
germ. buffer +30 μM decanal	928	18,600±340	55% [52%, 59%]	0.56±0.080
germ. buffer +30 μM decanal +0.4% fumarate	284	14,000±320	39% [35%, 43%]	0.32±0.14

428

429 **Table 1. Bioluminescence signal amplitude statistics.** Columns denote media, the number of
430 spores analyzed, and the statistics of n_g, the photon counts per spore integrated over the 12 h
431 after germination. The ± signs indicate 1 standard error. The bracketed interval in the coefficient
432 of variation column is the 95% confidence interval.

433

434 **Figure Legends**

435 **Fig. 1. Schematic of bioluminescence microscope and perfusion chamber with example**
436 **images and time series. (A)** Microscope schematic showing 3 light paths: bright field (blue),
437 luminescence (green), and autofocus infrared (red). For bright field imaging (blue path), the
438 external illumination is focused near the bottom of the agarose pad (yellow slab), where sample
439 cells are sandwiched against a glass coverslip. The sample emits luminescence (green path) in
440 all directions. A temperature-controlled, light-tight box (thick black lines) encloses the microscope.
441 **(B)** The perfusion chamber flows medium around the agarose pad (yellow) that traps sample cells
442 against a glass coverslip on the chamber bottom, sealed by an O-ring (orange). **(C)** Bright field
443 image of P_{sspB}-*luxABCDE* spores, before the addition of germinant (time 0 h). Highly refractile
444 dormant spores appear dark, *i.e.*, high contrast. The field of view contains approximately 900

445 spores. Scale bar: 20 μm. **(D,E)** The subregion bounded by the green box is shown in panels (D)
446 (bright field) and (E) (luminescence), showing the lack of luminescence signal from dormant
447 spores. **(F,G)** The same region is depicted 3.5 h after the addition of 100 μM L-alanine, showing
448 spores' typical loss of bright field contrast upon germination (F), and the corresponding increase
449 in luminescence signal (G) that occurs in some cells after germination. **(H,I)** Time series of bright
450 field contrast (H) and luminescent photon counts (I) of the 5 representative spores outlined in (D)-
451 (G). The rapid loss of contrast shown in panel (H) defines the time of germination, τ_g, for each
452 spore. Colored cell outlines are dilated by 1 pixel for visualization. Panel (D) scale bar: 5 μm.
453
454 **Fig. 2. Bioluminescence dynamics of spore populations germinating in response to L-**
455 **alanine. (A)** The bioluminescence emitted by P_{sspB}-*luxABCDE* spores germinating in a range of
456 L-alanine concentrations was assayed in a 96-well plate reader. Each well contained
457 approximately 6×10^6 spores. Lines depict the mean signal over 3 replicates; the standard
458 deviation was negligible on this scale. **(B)** The bioluminescence signal $\phi(t)$ was measured in
459 individual spores germinating in response to various concentrations of L-alanine added at time 0
460 h. The mean signal over all spores (>600 individuals per concentration) is plotted at each time
461 point. **(C)** The bioluminescence signals in (A) and (B) were integrated over the period between 0
462 and 12 h after the addition of alanine to calculate the population-averaged photon counts n,
463 plotted as a function of alanine concentration.
464
465 **Fig. 3. Time of germination varies in populations and synchronizes with bioluminescence**
466 **dynamics.** Dormant spores were exposed to 5 concentrations of L-alanine at time 0 h. **(A)** The
467 fraction of spores that had not yet germinated by time t, $P(\tau_g>t)$, is plotted on a linear scale (left)
468 and a log scale (right). An offset is added to avoid divergence of zero values on the log scale. **(B)**
469 The luminescence signal of each spore as a function of time elapsed since the time of germination
470 is $\phi_g(t) = \phi(t-\tau_g)$, defined for spores that germinated during the acquisition interval. The population

471 average of $\phi_g(t)$ is plotted for each concentration of L-alanine. Note that no spores germinated in
472 1 μM L-alanine and so no curve for that condition appears in (B).
473
474 **Fig. 4. Variability in bioluminescence dynamics over spores. (A)** Bioluminescence as a
475 function of time since germination is analyzed in terms of variability over individuals. Data include
476 all spores that germinated in response to L-alanine at 4 concentrations (Table 1). The time series
477 of $\phi_g(t)$ for a randomly chosen subset of 500 cells are plotted as thin black lines. The solid red line
478 indicates the median over the 11,000 cells comprising the data set, and the dashed red lines
479 indicate the 16% and 84% quartiles. (**B-E**) Principal component analysis was performed on time
480 series $\phi_g(t)$ from 4 experimental conditions: germination buffer only (B), 0.4% sodium fumarate
481 (C), 30 μM decanal (D), and 30 μM decanal plus 0.4% sodium fumarate (E). The dark gray line
482 shows the population average $\langle\phi_g(t)\rangle$ for each condition. The first principal component for each
483 condition explained 30%, 55%, 68%, and 58% of the total variance, respectively. The red line
484 shows the loadings of the first principle component, *i.e.*, $\lambda_1^{1/2}w_1(t)$, where λ_1 is the largest
485 eigenvalue of the covariance matrix, and w_1 is the first principle component, scaled to unit norm.
486 The average and loadings are plotted on separate axes. The first principal component and the
487 population average were highly correlated in all conditions: defining $r=\mathrm{cor}(w_1(t),\langle\phi_g(t)\rangle)$, $r_{\text{buffer-}}$
488 $_{\text{only}}$=84%, r_{fumarate}=97%, r_{decanal}=89%, $r_{\text{decanal+fumarate}}$=99% (all p-values $<2.2\times10^{-16}$).
489

490 **Figures**

491

492 **Figure 1**

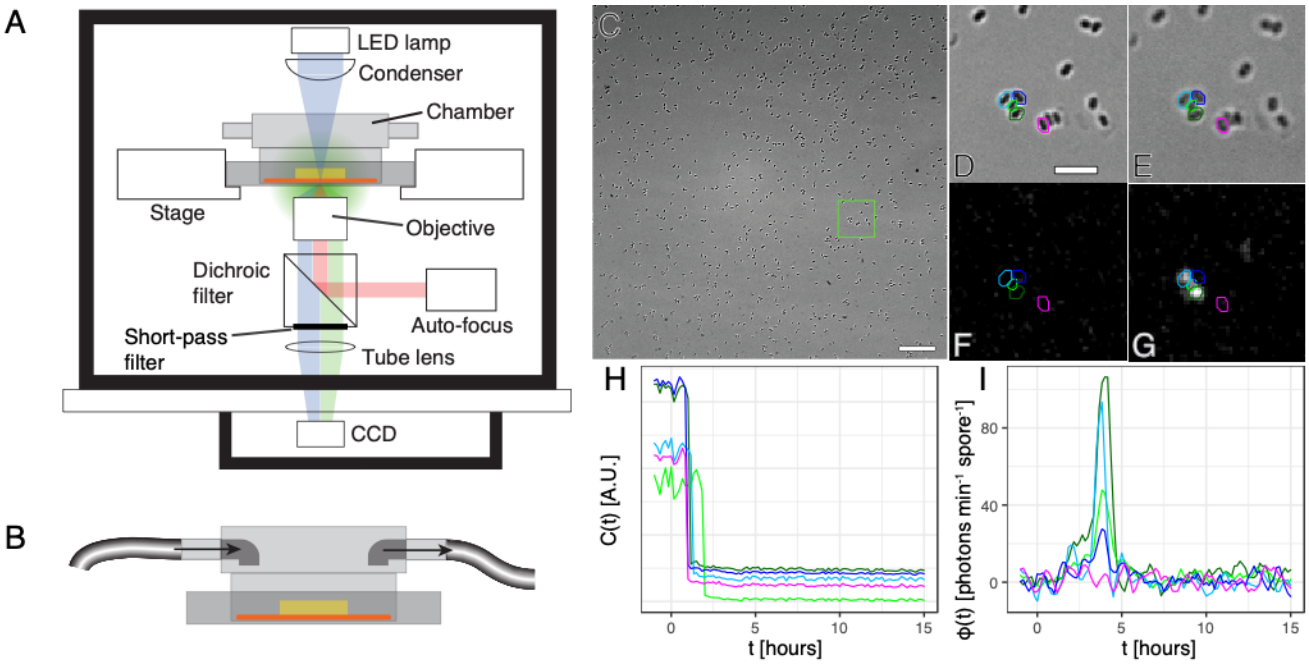

493

494

495 **Figure 2**

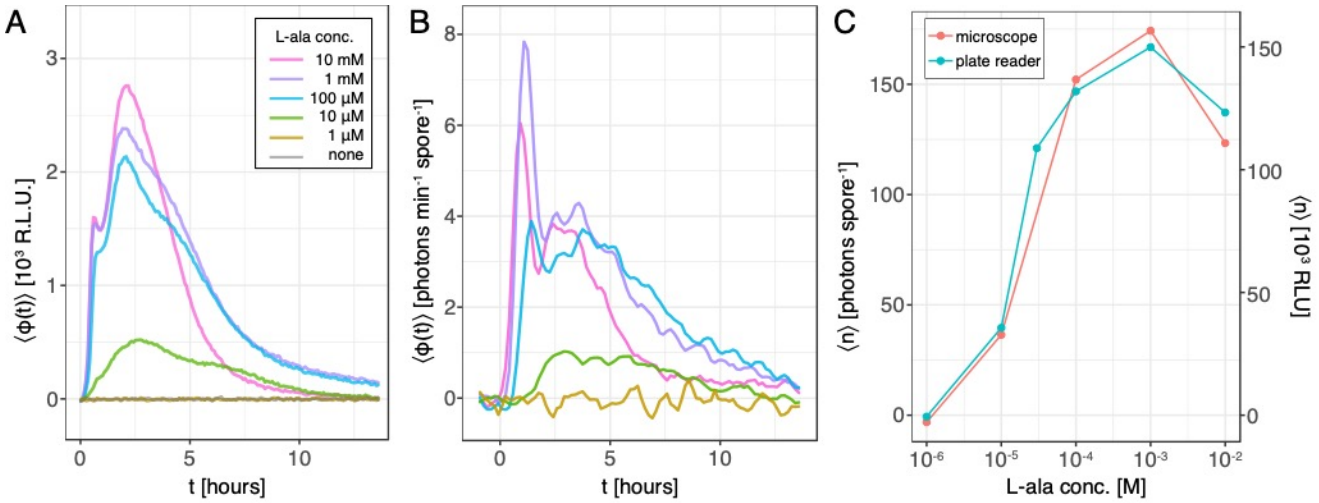

496

497

498 **Figure 3**

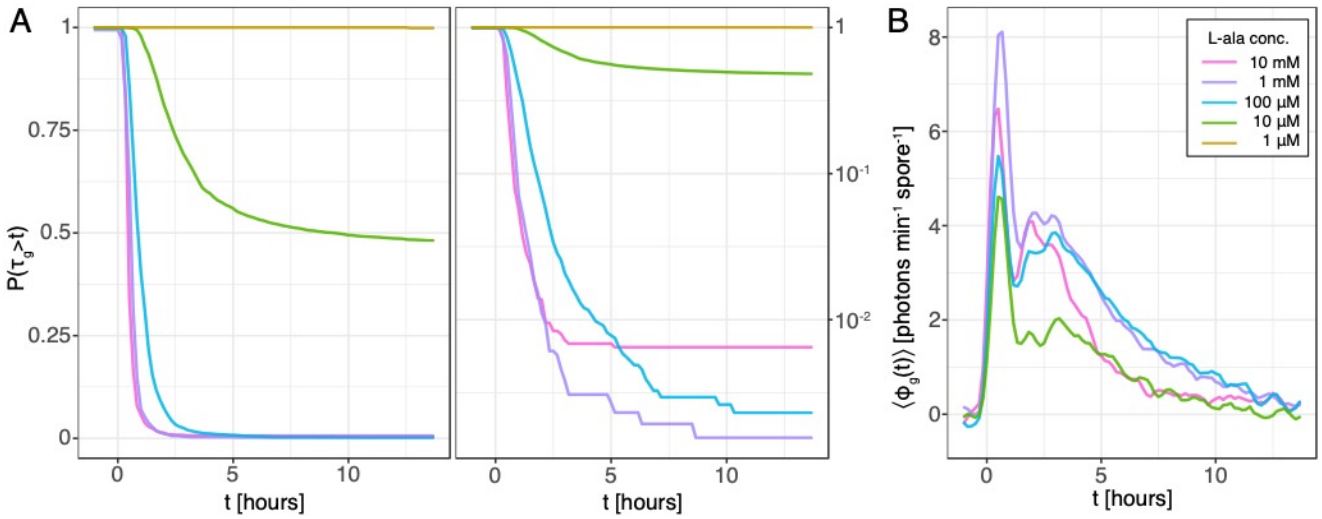

499

500

501 **Figure 4**

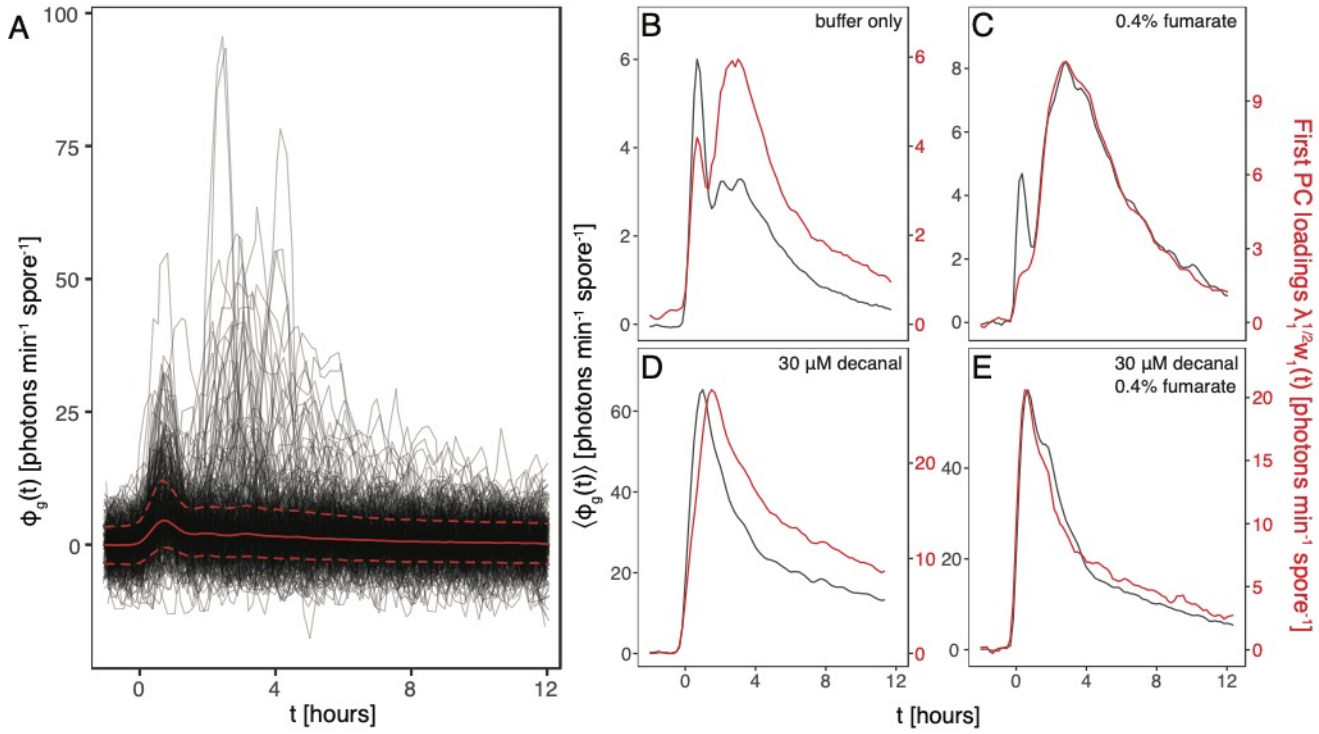

502
503

References

1. Setlow, P., *Spores of Bacillus subtilis: their resistance to and killing by radiation, heat and chemicals.* Journal of Applied Microbiology, 2006. **101**(3): p. 514-525.
2. Graham-Smith, G.S., *The longevity of dry spores of B. anthracis.* Journal of Hygiene, 1930. **30**(2): p. 213-215.
3. Sneath, P.H.A., *Longevity of micro-organisms.* Nature, 1962. **195**(4842): p. 643-646.
4. Desser, H. and E. Broda, *Radiochemical investigation of the respiration of spores of Bacillus cereus.* Archiv Für Mikrobiologie, 1969. **65**(1): p. 76-86.
5. Mehta, P. and D.J. Schwab, *Energetic costs of cellular computation.* Proceedings of the National Academy of Sciences of the United States of America, 2012. **109**(44): p. 17978-17982.
6. Xue, B.K., P. Sartori, and S. Leibler, *Environment-to-phenotype mapping and adaptation strategies in varying environments.* Proceedings of the National Academy of Sciences of the United States of America, 2019. **116**(28): p. 13847-13855.
7. Yi, X., J. Liu, J.R. Faeder, and P. Setlow, *Synergism between different germinant receptors in the germination of Bacillus subtilis spores.* Journal of Bacteriology, 2011. **193**(18): p. 4664-4671.
8. Veening, J.-W., E.J. Stewart, T.W. Berngruber, F. Taddei, O.P. Kuipers, and L.W. Hamoen, *Bet-hedging and epigenetic inheritance in bacterial cell development.* Proceedings of the National Academy of Sciences of the United States of America, 2008. **105**(11): p. 4393-4398.
9. Mutlu, A., S. Trauth, M. Ziesack, K. Nagler, J.P. Bergeest, K. Rohr, N. Becker, T. Höfer, and I.B. Bischofs, *Phenotypic memory in Bacillus subtilis links dormancy entry and exit by a spore quantity-quality tradeoff.* Nature Communications, 2018. **9**.

529 10. Zhang, J.-Q., K.K. Griffiths, A. Cowan, P. Setlow, and J. Yu, *Expression level of Bacillus*
530 *subtilis germinant receptors determines the average rate but not the heterogeneity of*
531 *spore germination.* Journal of Bacteriology, 2013. **195**(8): p. 1735-1740.
532 11. Powell, J.F. and R.E. Strange, *Biochemical changes occurring during the germination of*
533 *bacterial spores.* Biochemical Journal, 1953. **54**(2): p. 205-209.
534 12. Sturm, A. and J. Dworkin, *Phenotypic diversity as a mechanism to exit cellular dormancy.*
535 Curr Biol, 2015. **25**(17): p. 2272-2277.
536 13. de Jong, I.G., J.-W. Veening, and O.P. Kuipers, *Heterochronic phosphorelay gene*
537 *expression as a source of heterogeneity in Bacillus subtilis spore formation.* Journal of
538 Bacteriology, 2010. **192**(8): p. 2053-2067.
539 14. Takhaveev, V. and M. Heinemann, *Metabolic heterogeneity in clonal microbial*
540 *populations.* Current Opinion in Microbiology, 2018. **45**: p. 30-38.
541 15. Laflamme, C., D. Verreault, S. Lavigne, L. Trudel, J. Ho, and C. Duchaine,
542 *Autofluorescence as a viability marker for detection of bacterial spores.* Frontiers in
543 Bioscience, 2005. **10**: p. 1647-1653.
544 16. Sarasanandarajah, S., J. Kunnil, B.V. Bronk, and L. Reinisch, *Two-dimensional*
545 *multiwavelength fluorescence spectra of dipicolinic acid and calcium dipicolinate.* Applied
546 Optics, 2005. **44**(7): p. 1182-1187.
547 17. Jelen, B.I., D. Giovannelli, and P.G. Falkowski, *The role of microbial electron transfer in*
548 *the coevolution of the biosphere and geosphere.* The Annual Review of Microbiology,
549 2016. **70**: p. 45-62.
550 18. Kim, B.H. and G.M. Gadd, *Bacterial Physiology and Metabolism*. 2008, Cambridge:
551 Cambridge University Press.
552 19. Gross, B.J. and M.Y. El-Naggar, *A combined electrochemical and optical trapping platform*
553 *for measuring single cell respiration rates at electrode interfaces.* Review of Scientific
554 Instruments, 2015. **86**(6).

555 20. Hastings, J.W., *Chemistries and colors of bioluminescent reactions: A review.* Gene, 1996.
556 **173**(1): p. 5-11.
557 21. Koga, K., T. Harada, H. Shimizu, and K. Tanaka, *Bacterial luciferase activity and the*
558 *intracellular redox pool in Escherichia coli.* Molecular Genetics and Genomics, 2005.
559 **274**(2): p. 180-188.
560 22. Carmi, O.A., G.S.A.B. Stewart, S. Ulitzur, and J. Kuhn, *Use of bacterial luciferase to*
561 *establish a promoter probe vehicle capable of nondestructive real-time analysis of gene*
562 *expression in Bacillus spp.* Journal of Bacteriology, 1987. **169**(5): p. 2165-2170.
563 23. Hill, P.J., L. Hall, D.A. Vinicombe, C.J. Soper, P. Setlow, W.M. Waites, S. Denyer, and
564 G.S.A.B. Stewart, *Bioluminescence and spores as biological indicators of inimical*
565 *processes.* Journal of Applied Bacteriology, 1994. **76**: p. S129-S134.
566 24. Schmalisch, M., E. Maiques, L. Nikolov, A.H. Camp, B. Chevreux, A. Muffler, S.
567 Rodriguez, J. Perkins, and R. Losick, *Small genes under sporulation control in the Bacillus*
568 *subtilis genome.* Journal of Bacteriology, 2010. **192**(20): p. 5402-5412.
569 25. Ciarciaglini, G., P.J. Hill, K. Davies, P.J. McClure, D. Kilsby, M.H. Brown, and P.J. Coote,
570 *Germination-induced bioluminescence, a route to determine the inhibitory effect of a*
571 *combination preservation treatment on bacterial spores.* Applied and Environmental
572 Microbiology, 2000. **66**(9): p. 3735-3742.
573 26. Hastings, J.W. and G. Weber, *Total quantum flux of isotropic sources.* Journal of the
574 Optical Society of America, 1963. **53**(12): p. 1410-1415.
575 27. Gregor, C., K.C. Gwosch, S.J. Sahl, and S.W. Hell, *Strongly enhanced bacterial*
576 *bioluminescence with the ilux operon for single-cell imaging.* Proceedings of the National
577 Academy of Sciences of the United States of America, 2018. **115**(5): p. 962-967.
578 28. Mihalcescu, I., W. Hsing, and S. Leibler, *Resilient circadian oscillator revealed in individual*
579 *cyanobacteria.* Nature, 2004. **430**(6995): p. 81-85.

580 29. Phiefer, C.B., R.J. Palmer, and D.C. White, *Comparison of relative photon flux from single*
581 *cells of the bioluminescent marine bacteria Vibrio fischeri and Vibrio harveyi using photon-*
582 *counting microscopy.* Luminescence, 1999. **14**(3): p. 147-151.
583 30. McLean, I.S., *Electronic Imaging in Astronomy: Detectors and Instrumentation*. 2008:
584 Springer Science & Business Media.
585 31. Zhang, P., L. Kong, G. Wang, M. Scotland, S. Ghosh, B. Setlow, P. Setlow, and Y.-Q. Li,
586 *Analysis of the slow germination of multiple individual superdormant Bacillus subtilis*
587 *spores using multifocus Raman microspectroscopy and differential interference contrast*
588 *microscopy.* Journal of Applied Microbiology, 2012. **112**(3): p. 526-536.
589 32. Cabrera-Martinez, R.-M., F. Tovar-Rojo, V.R. Vepachedu, and P. Setlow, *Effects of*
590 *overexpression of nutrient receptors on germination of spores of Bacillus subtilis.* Journal
591 of Bacteriology, 2003. **185**(8): p. 2457-2464.
592 33. Weare, B.C., A.R. Navato, and R.E. Newell, *Empirical orthogonal analysis of Pacific sea*
593 *surface temperatures.* Journal of Physical Oceanography, 1976. **6**(5): p. 671-678.
594 34. Scott, I.R. and D.J. Ellar, *Metabolism and the triggering of germination of Bacillus*
595 *megaterium. Use of L-[3H]alanine and tritiated water to detect metabolism.* Biochemical
596 Journal, 1978. **174**(2): p. 635-640.
597 35. Soly, R.R. and E.A. Meighen, *Identification of the acyl transfer site of fatty acyl-protein*
598 *synthetase from bioluminescent bacteria.* Journal of Molecular Biology, 1991. **219**(1): p.
599 69-77.
600 36. Paidhungat, M., K. Ragkousi, and P. Setlow, *Genetic requirements for induction of*
601 *germination of spores of Bacillus subtilis by Ca2+-dipicolinate.* Journal of Bacteriology,
602 2001. **183**(16): p. 4886-4893.
603 37. Huang, S.-S., D. Chen, P.L. Pelczar, V.R. Vepachedu, P. Setlow, and Y.-Q. Li, *Levels of*
604 *Ca(2+)-dipicolinic acid in individual Bacillus spores determined using microfluidic Raman*
605 *tweezers.* Journal of Bacteriology, 2007. **189**(13): p. 4681-4687.

606 38. Schrödinger, E., *What is life? The physical aspect of the living cell and mind.* 1944,
607 Cambridge: Cambridge University Press.
608 39. Hoehler, T.M., *Biological energy requirements as quantitative boundary conditions for life*
609 *in the subsurface.* Geobiology, 2004. **2**(4): p. 205-215.
610 40. Morita, R.Y., *Bacteria in Oligotrophic Environments*. 1997, New York: Chapman & Hall.
611 41. Price, P.B. and T. Sowers, *Temperature dependence of metabolic rates for microbial*
612 *growth, maintenance, and survival.* Proceedings of the National Academy of Sciences of
613 the United States of America, 2004. **101**(13): p. 4631-4636.
614 42. Lever, M.A., K.L. Rogers, K.G. Lloyd, J. Overmann, B. Schink, R.K. Thauer, T.M. Hoehler,
615 and B.B. Jørgensen, *Life under extreme energy limitation: a synthesis of laboratory- and*
616 *field-based investigations.* FEMS Microbiology Reviews, 2015. **39**(5): p. 688-728.
617 43. Hoehler, T.M. and B.B. Jørgensen, *Microbial life under extreme energy limitation.* Nature
618 Reviews Microbiology, 2013. **11**(2): p. 83-94.
619 44. Nelson, D.L. and A. Kornberg, *Biochemical studies of bacterial sporulation and*
620 *germination. XIX. Phosphate metabolism during sporulation.* The Journal of Biological
621 Chemistry, 1970. **245**(5): p. 1137-1145.
622 45. Swerdlow, B.M., B. Setlow, and P. Setlow, *Levels of H+ and other monovalent cations in*
623 *dormant and germinating spores of Bacillus megaterium.* Journal of Bacteriology, 1981.
624 **148**(1): p. 20-29.
625 46. Singh, R.P., B. Setlow, and P. Setlow, *Levels of small molecules and enzymes in the*
626 *mother cell compartment and the forespore of sporulating Bacillus megaterium.* Journal of
627 Bacteriology, 1977. **130**(3): p. 1130-1138.
628 47. Ghosh, S., G. Korza, M. Maciejewski, and P. Setlow, *Analysis of metabolism in dormant*
629 *spores of Bacillus species by 31P nuclear magnetic resonance analysis of low-molecular-*
630 *weight compounds.* Journal of Bacteriology, 2015. **197**(5): p. 992-1001.

631 48. Matheson, I.B.C. and J. Lee, *Kinetics of bacterial bioluminescence and the fluorescent*
632 *transient.* Photochemistry and Photobiology, 1983. **38**(2): p. 231-240.
633 49. Sapru, V. and T.P. Labuza, *Glassy state in bacterial spores predicted by polymer glass-*
634 *transition theory.* Journal of Food Science, 1993. **58**(2): p. 445-448.
635 50. Ablett, S., A.H. Darke, P.J. Lillford, and D.R. Martin, *Glass formation and dormancy in*
636 *bacterial spores.* International Journal of Food Science and Technology, 1999. **34**(1): p.
637 59-69.
638 51. Hagen, S.J., J. Hofrichter, and W.A. Eaton, *Protein reaction kinetics in a room-temperature*
639 *glass.* Science, 1995. **269**(5226): p. 959-962.
640 52. Sunde, E.P., P. Setlow, L. Hederstedt, and B. Halle, *The physical state of water in bacterial*
641 *spores.* Proceedings of the National Academy of Sciences of the United States of America,
642 2009. **106**(46): p. 19334-19339.
643

Supporting Materials and Methods

Sensitivity limits of bioluminescence microscopy

Sensor read noise, dark current, and high energy particles such as cosmic rays generate a noise background for imaging. The signal measured from a steadily emitting source accumulates with increasing exposure time t. Noise due to dark current also accumulates with t, but modern cooled CCDs have very low dark current, so that sensor read noise dominates for t up to about 1 h. The number of high energy particle artifacts per image also increases with t. These artifacts can be identified automatically [1], so that pixels affected by these artifacts can be removed from subsequent analysis. From a practical perspective, t must be short enough to ensure that the majority of pixels are not affected by these artifacts. The flux of high energy particles from cosmic rays is about 1 cm^{-2} min^{-1} [1]. In our preliminary experiments, artifacts from high energy particles limited t to 10 min.

After removing artifacts due to high energy particles, imaging noise is dominated by sensor readout noise. We consider the following parameters: the average rate of photon emission per spore, ψ; the average number of pixels in the luminescence image of a spore, N; the RMS readout noise per pixel σ_r; the exposure time t, and the collection efficiency of the imaging setup s. Note that the collection efficiency s is the ratio of the number of emitted photons to the number of electrons measured by the sensor. It includes geometric effects, *i.e.*, losses due to the collection geometry, reflections from optical surfaces, and the quantum yield of the sensor.

The signal to noise ratio for each pixel in the image of the spore, χ_p, is the number of electrons per pixel per exposure arising from emitted luminescence, divided by the magnitude of the readout noise: $\chi_p = s\psi t N^{-1}\sigma_r^{-1}$. The signal from each spore is the sum over the signals from the pixels comprising its image. The readout noise is independent for each pixel, so the signal to noise ratio per spore, χ, equals $\chi_p N^{1/2} = s\psi t N^{-1/2}\sigma_r^{-1}$. The sensitivity limit of the technique is taken to be the rate of photon emission per spore for which the signal to noise ratio χ is equal to 1: $\psi_{min} = s^{-1}t^{-1}N^{1/2}\sigma_r$.

Optimizing the sensitivity of the technique amounts to maximizing collection efficiency s, minimizing the number of pixels per spore n, and minimizing the sensor read noise σ_r. Practically, s is less than 1/2 electrons per photon, since at least half of photons are emitted away from the collection objective. The numerical aperture of the objective should be as high as possible, to maximize collection of the remaining photons. The quantum efficiency of back-illuminated CCDs in the spectral range of bacterial bioluminescence (~490 nm) typically exceeds 0.9 electrons per photon. Accounting for these effects, we estimated that we could achieve a value of s as high as 0.3 electrons per photon. For the camera we used in the microscope, the parameters were as follows: s = 0.3 e^- photon^{-1} (estimated), t = 10 min, N = 10 pixels, σ_r = 3.6 e^-, which determines the sensitivity limit $\psi_{min} \approx$ 3.8 photons min^{-1}. Published results typically report the number of measured photons per time ($\gamma^{-1}s\psi$, where γ is the gain, expressed in electrons per photon), rather than the number emitted per time (ψ), and so we introduce a new symbol for the former rate: $\Phi = \gamma^{-1}s\psi$, and estimate the sensitivity limit $\Phi_{min} = \gamma^{-1}s\psi_{min} \approx$ 1 photons min^{-1} (γ = 1 e^- photon^{-1} for our setup).

We analyzed the signal to noise ratio of our measurements on a per-spore basis. The noise background was quantified by considering the statistics of luminescence signal from the reported experiments in regions of the image that did not contain spores. These regions were defined to each include the same number of pixels as a real spore. Twelve thousand such regions were analyzed, and the standard deviation of the estimated photon counts from each region was calculated: σ = 3.5 photons min^{-1}. The bioluminescence dynamics per spore $\Phi(t)$ varied over time and across spores. Detection of the signal from a particular spore is primarily determined by that spore's maximal signal. For the purposes of determining a single signal to noise ratio that would describe the typical sensitivity of the technique, we calculated the population-average of the temporal maximum bioluminescence signal:

$$\phi^* = \langle \max_t \phi(t) \rangle$$

The signal to noise ratio is given by $\chi = \Phi^{*}\sigma^{-1}$. Its values were χ = 4.2 (germination buffer only), 5.1 (0.4% fumarate), 22 (30 μM decanal), and 18 (30 μM decanal + 0.4% fumarate).

Image analysis

Background subtraction

Spatial inhomogeneities were observed in long exposure images, even those acquired in complete darkness without a luminescent sample. These inhomogeneities were found to be nearly constant over time and were treated as a form of background. To remove this background, a sequence of at least 20 images was acquired in darkness prior to each experiment, and the temporal median of this sequence, *i.e.*, the estimated background, was subtracted from each luminescence image subsequently acquired during the experiment.

Removal of artifacts due to high energy particles

Each luminescence image included several small regions of extremely bright pixels, due to high energy particles, such as cosmic rays, ionizing the CCD. In order to prevent these artifacts from corrupting the luminescence signal, we developed a routine to automatically detect pixels that appeared to be affected by such events. Pixels affected by artifacts had a particularly identifying feature: extreme brightness, that appeared rapidly in time and with very high spatial contrast. Temporal and spatial high-pass filters were applied to the images, and the resulting images were segmented, using a threshold chosen to separate the vast majority (>99%) of affected pixels from unaffected pixels. The affected regions were grown by 2 pixels to avoid any remaining signal contamination. The mean number of artifacts was 2.0 min^{-1}, and the mean number of pixels affected by each artifact was 28.

Spore identification and segmentation

Spores were identified by determining the maximally stable extremal regions of the bright field image, using the VLFeat software library [2, 3]. The parameters of the method were tuned manually to identify >99% of spores, with a negligible false identification rate (<0.1%).

Determination of Germination Time τ_g

The bright field contrast of each spore was determined by calculating the spatial gradient of each bright field image, ∇I_{BF}. The magnitude of the gradient was averaged over the pixels p corresponding to each spore to calculate its contrast:

$$C(t) = \sum_{p} \|\nabla I_{\mathrm{BF}}(t)\|^2$$

The dynamics of contrast of germinating spores typically appeared as noisy step function, declining from a high value prior to germination to a low value after. The time of germination τ_g was determined for each spore by fitting the measured contrast with a regression tree having a single split, using the rpart package for R, v. 4.1-15. The automatically determined τ_g was found to exactly match the value determined by manually considering the time-lapse images in 100 spores selected randomly from 4 data sets.

Statistical analysis

Temporal filtering

Camera read noise and photon counting noise (shot noise) corrupt the counts of bioluminescence photons. Each of the noise sources is expected to have zero temporal autocorrelation, while the bioluminescence dynamics are expected to have significant autocorrelation. Defining the photon counts within each pixel p as $X_p(t)$, we expect the power spectral density of X_p to be different for pixels located within the image of a spore vs. pixels located outside (background). To text this, we estimated the power spectral density of $X_p(t)$ over 110,000 pixels within the image of spores ("signal": $P_S(\omega)$) and over 200,000 pixels not within the image of spores (background: $P_{BG}(\omega)$).

The power spectral density of the background was flat, while that of the signal was flat above $\omega \approx 0.84\ \mathrm{h}^{-1}$. In order to filter the background noise without significantly blurring the signal dynamics, we applied a low-pass filter (sinc filter), with a cutoff period of 36 min, to the bioluminescence signal measured from each pixel. For each spore, the sum of these counts over all pixels inside its bright field image was calculated for each time point, resulting in $\Phi(t)$.

Principal component analysis

The covariance matrix $C(s,t)$ was calculated over all germinating spores as:

$$C(s,t) = N^{-1} \sum_{i=1}^{N} \left(\phi_{\mathrm{g}}^{i}(s) - \langle \phi_{\mathrm{g}}(s) \rangle\right)\left(\phi_{\mathrm{g}}^{i}(t) - \langle \phi_{\mathrm{g}}(t) \rangle\right)$$

where $\phi^{i}_{\mathrm{g}}(t)$ is the estimated rate of photons counted from spore i at time t, and N is the number of spores in the data set. The times s and t took values corresponding to 87 time points: 12 before germination (2 h), and 75 following germination (12.3 h). Principal component analysis was performed on the covariance matrix $C(s,t)$, resulting in the eigenvalues λ_i and the eigenvectors $w_i(t)$. The eigenvalues have units (photons $\mathrm{min}^{-1})^2$ and the eigenvectors are unitless and have norm 1:

$$\sum_{j=1}^{87} \left(w_i(t_j)\right)^2 = 1$$

The temporal pattern of variation explained by mode i is quantified by $\lambda_i^{1/2} w_i(t)$, as is plotted in Figs. 4B-E for $i = 1$.

Statistics of n_{g}

The number of photons counted per spore was calculated as

$$n_{\mathrm{g}} = \sum_{t \geq 0}^{t \leq 12\ \mathrm{h}} \phi_{\mathrm{g}}(t) \Delta t$$

where $\Delta t = 10$ min is the exposure time.

For Table 1, the estimates of the skew of n_g and its standard error were calculated for each data set using method 3 of Joanes & Gill [4]. The confidence interval of the coefficient of variation was estimated using the formula of McKay [5].

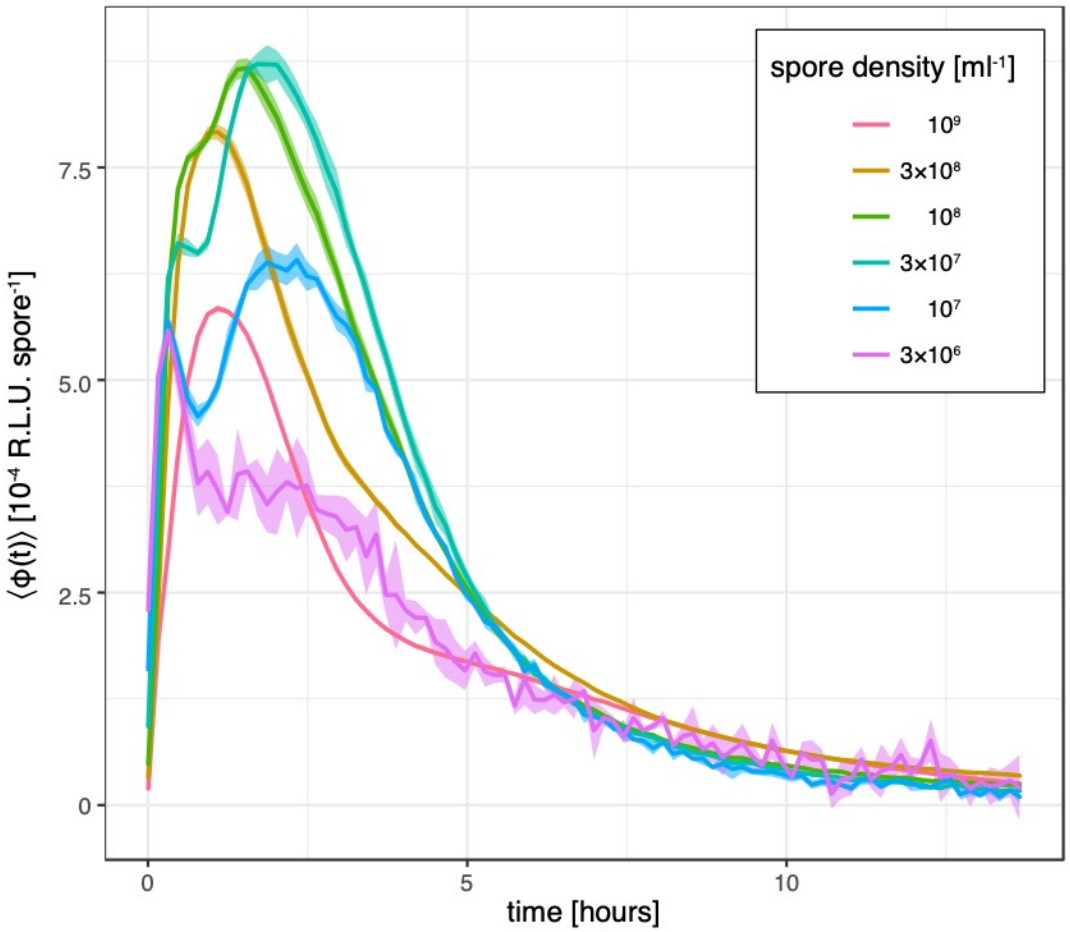

Figure S1. Bioluminescence dynamics depend on spore concentration. The population-averaged bioluminescence signal $\langle \phi(t) \rangle$ was measured in a 96-well plate reader, at a range of spore densities, and normalized by the number of spores per well to facilitate comparison between densities. Spores were induced to germinate with 1 mM L-alanine. Lines depict the mean signal over 3 replicates and the shaded region encloses ±1 standard deviation. Spore density in the experiments performed with the microscope was less than 10^5 ml^{-1}.

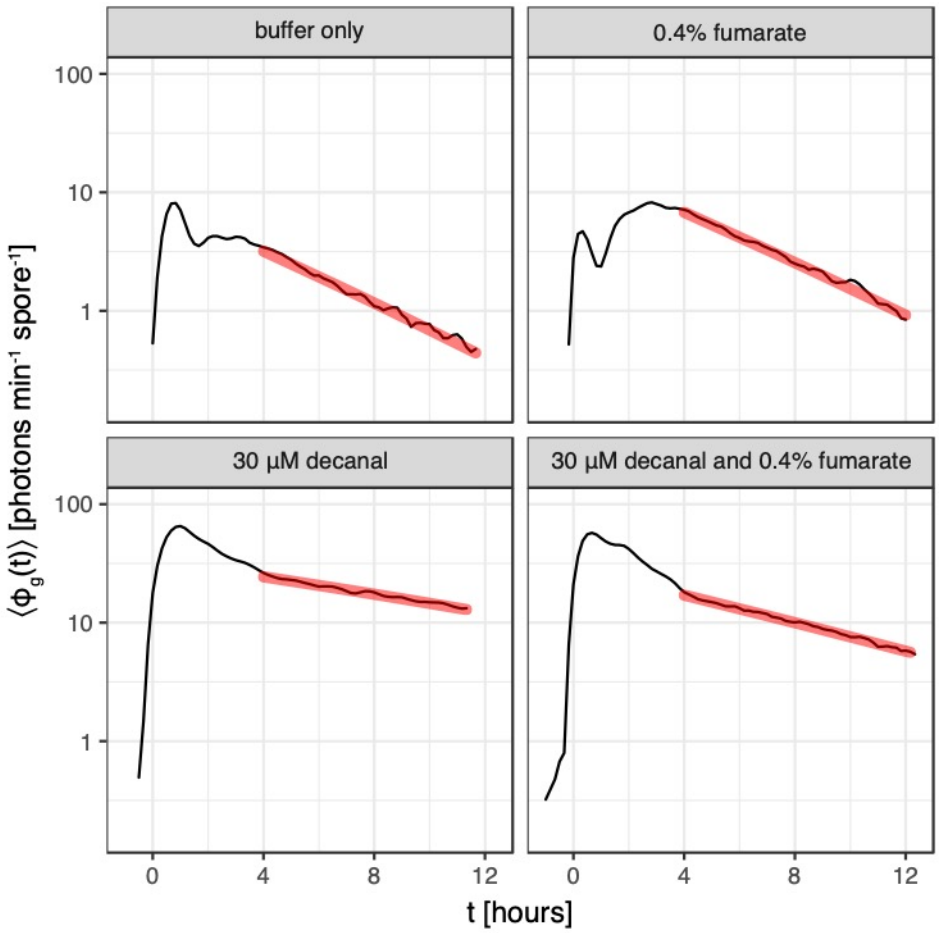

Figure S2. Bioluminescence signal decays exponentially after 4 h post-germination. The population-averaged bioluminescence dynamics of germinating spores $\langle \phi_g(t) \rangle$, depicted by the black line, exhibit exponential decline, beginning at 4 h post-germination. The rate of exponential decline r was estimated in each of 4 conditions: $r_{\text{buffer-only}}$ = 22% h^{-1}, r_{fumarate} = 22% h^{-1}, r_{decanal} = 8% h^{-1}, $r_{\text{decanal+fumarate}}$ = 12% h^{-1}. Estimated fits are depicted by red lines.

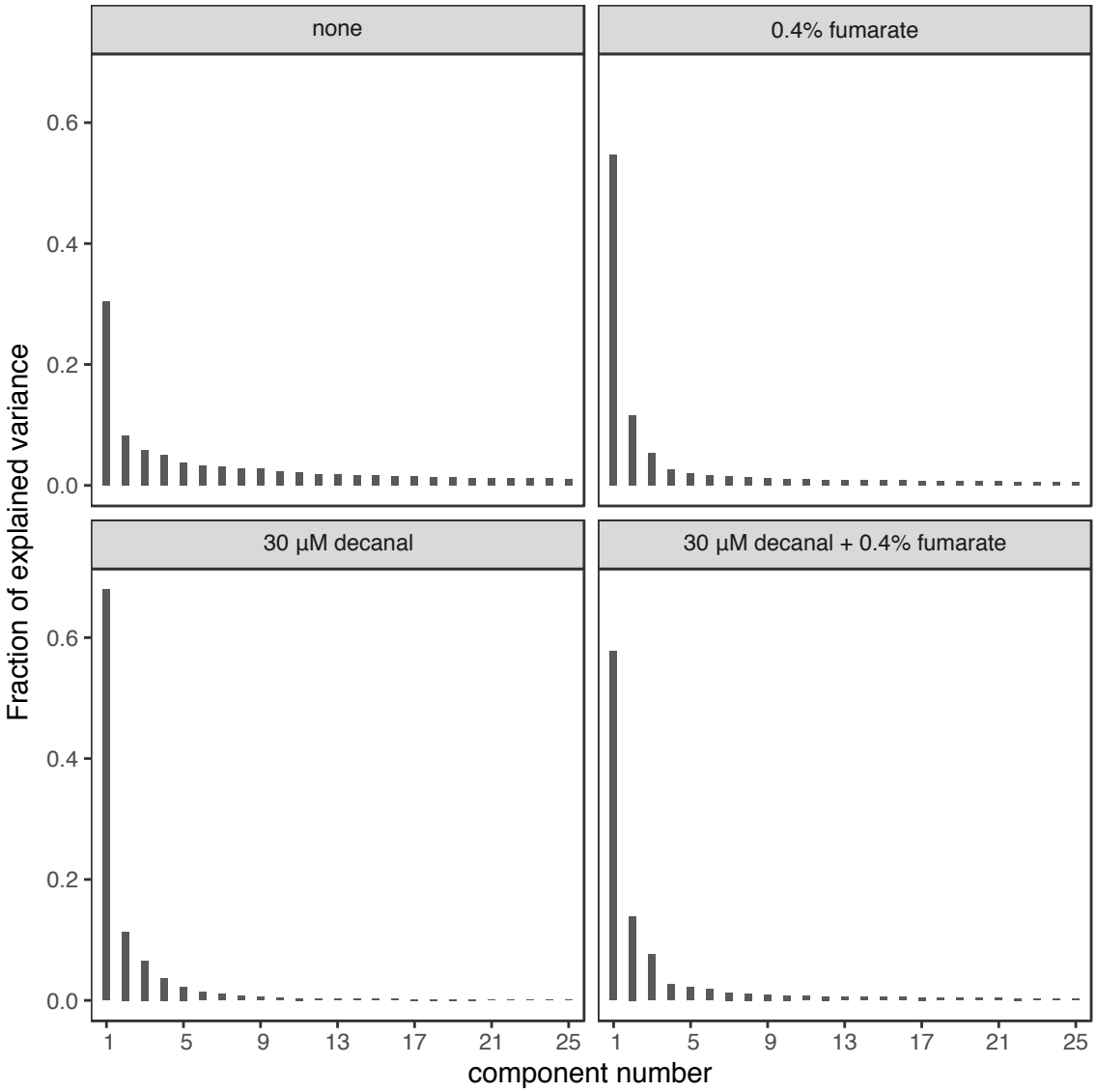

Figure S3. Variance explained by principal components. Principal component analysis was performed on the bioluminescent photon counts $\phi_g(t)$ for each of 4 experimental conditions, as described in the Results section. The variance explained by principal component number k is λ_k, and the fraction of variance explained is $\lambda_k(\Sigma_i \lambda_i)^{-1}$. The data sets included 87 time points and therefore 87 principal components; only the first 25 components are included in the plots.

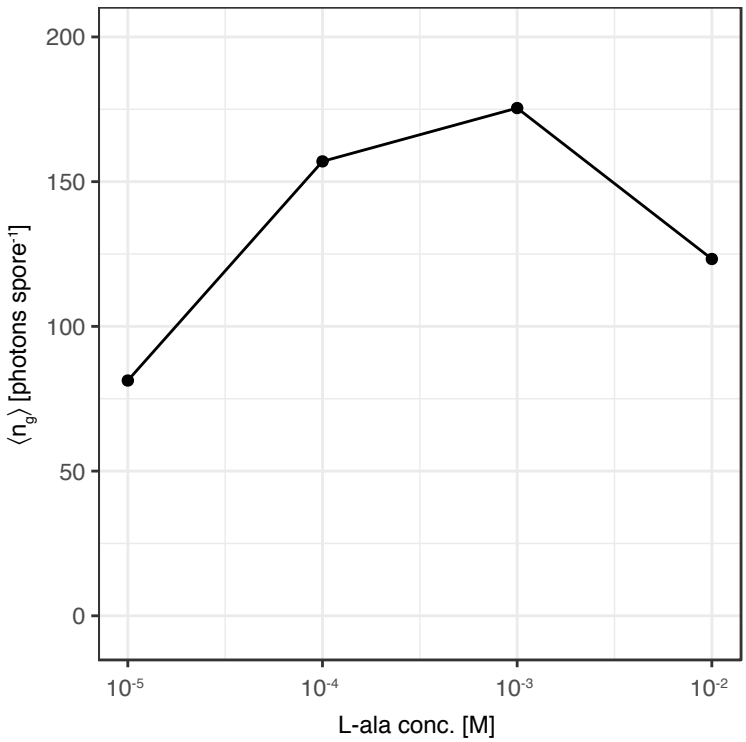

Figure S4. Bioluminescent photons counted per germinating spore. The bioluminescence signal as a function of time since germination, $\phi_g(t) = \phi(t\text{-}\tau_g)$, was integrated from 0 to 12 h post-germination to calculate the number of photons counted per germinating spore, n_g. The average of n_g over all germinating spores is plotted against L-alanine concentration.

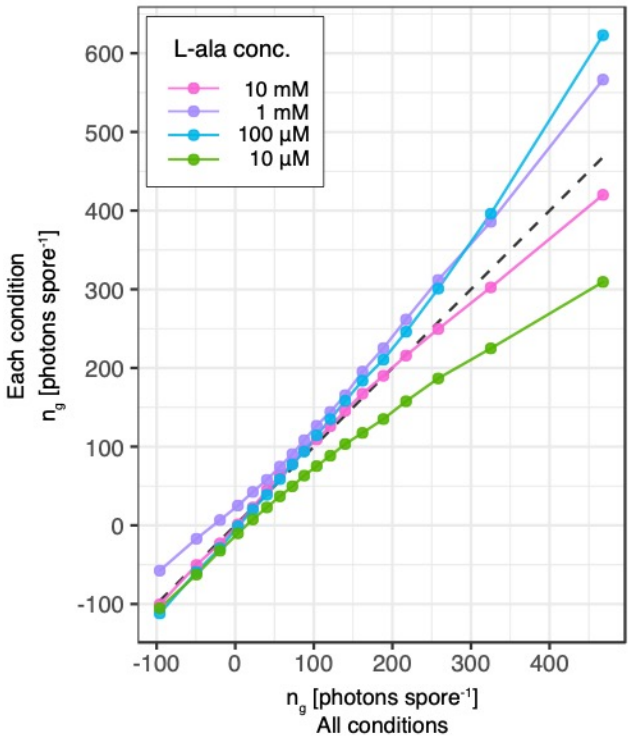

Figure S5. Quantile-quantile plot of bioluminescent photons counted per spore, germinating in response to 4 concentrations of L-alanine. Quantiles of the number of photons emitted per germinating spore during the 12 h post-germination, n_g, were determined for 4 concentrations of L-alanine. Quantiles were also calculated for the data from all 4 L-alanine concentrations, weighted for equal contribution from each condition. The quantiles in each condition are plotted on the vertical axis, as a function of the corresponding quantile in all conditions. Quantiles were determined in increments of 5%, starting at 5% and ending at 95%.

References

1. Groom, D., *Cosmic rays and other nonsense in astronomical CCD imagers.* Experimental Astronomy, 2002. **14**(1): p. 45-55.
2. Matas, J., O. Chum, M. Urban, and T. Pajdla, *Robust wide-baseline stereo from maximally stable extremal regions.* Image and Vision Computing, 2004. **22**(10): p. 761-767.
3. Vedaldi, A.F., B., *VLFeat: an open and portable library of computer vision algorithms*. 2008: http://www.vlfeat.org/.
4. Joanes, D.N. and C.A. Gill, *Comparing measures of sample skewness and kurtosis.* Journal of the Royal Statistical Society Series D (The Statistician), 1998. **47**(1): p. 183-189.
5. McKay, A.T., *Distribution of the coefficient of variation and the extended "t" distribution.* Journal of the Royal Statistical Society, 1932. **95**(4): p. 695-698.